The nonmotor adaptor HMMR dampens Eg5-mediated forces to preserve the kinetics and integrity of chromosome segregation

Helen Chen[a], Marisa Connell[a], Lin Mei[a], Gregor S. D. Reid[a,b], and Christopher A. Maxwell[a,b,*]
[a]Department of Pediatrics, University of British Columbia, Vancouver, BC V5Z 4H4, Canada; [b]Michael Cuccione Childhood Cancer Research Program, BC Children's Hospital, Vancouver, BC V5Z 4H4, Canada

ABSTRACT **Mitotic spindle assembly and organization require forces generated by motor proteins. The activity of these motors is regulated by nonmotor adaptor proteins. However, there are limited studies reporting the functional importance of adaptors on the balance of motor forces and the promotion of faithful and timely cell division. Here we show that genomic deletion or small interfering RNA silencing of the nonmotor adaptor *Hmmr*/HMMR disturbs spindle microtubule organization and bipolar chromosome–kinetochore attachments with a consequent elevated occurrence of aneuploidy. Rescue experiments show a conserved motif in HMMR is required to generate interkinetochore tension and promote anaphase entry. This motif bears high homology with the kinesin Kif15 and is known to interact with TPX2, a spindle assembly factor. We find that HMMR is required to dampen kinesin Eg5-mediated forces through localizing TPX2 and promoting the formation of inhibitory TPX2-Eg5 complexes. In HMMR-silenced cells, K-fiber stability is reduced while the frequency of unattached chromosomes and the time needed for chromosome segregation are both increased. These defects can be alleviated in HMMR-silenced cells with chemical inhibition of Eg5 but not through the silencing of Kif15. Together, our findings indicate that HMMR balances Eg5-mediated forces to preserve the kinetics and integrity of chromosome segregation.**

Monitoring Editor
Xueliang Zhu
Chinese Academy of Sciences

Received: Aug 25, 2017
Revised: Jan 19, 2018
Accepted: Jan 25, 2018

INTRODUCTION

The formation and function of a bipolar mitotic spindle requires forces generated by motor proteins that act along microtubules to stabilize the spindle and to capture, align, and segregate chromosomes. The kinesin motors kinesin-5 (Eg5) and kinesin-12 (Kif15/hklp2) generate outward-directed forces that are antagonized by inward-directed forces generated by the dynein complex, and this balance of opposing motor forces stabilizes the metaphase spindle (Sharp *et al.*, 2000). Motor force imbalance results in the formation of mono- and multipolar spindles, unfocused spindle poles, aberrant spindle organization, improper chromosome attachment, and delayed cell division kinetics, all of which could result in the failure of cell division and the production of aneuploid progeny cells (Sharp *et al.*, 2000; Tanenbaum *et al.*, 2008; Ferenz *et al.*, 2009; Daum *et al.*, 2012; van Heesbeen *et al.*, 2014). Harmonization of antagonistic motor activities can be achieved by dual inhibition of dynein and Eg5 or overexpression of Kif15 in the absence of Eg5 activity (Tanenbaum *et al.*, 2008, 2009; Ferenz *et al.*, 2009; van Heesbeen *et al.*, 2014). These studies highlight the importance of motor force balance to the timely and successful conclusion of cell division.

Physiological regulation of motor complexes relies on interactions with nonmotor adaptor proteins, which determine motor localization, movement, and cargo binding. For example, dynactin is a multisubunit adaptor complex that links dynein together with a microtubule and its cargo and enhances motor processivity in vitro (Kardon and Vale, 2009). At the spindle poles, the microtubule-associated, hyaluronan-mediated motility receptor (HMMR) protein interacts with the dynein motor complex to prevent spindle pole fragmentation (Maxwell *et al.*, 2003). Recently, HMMR was shown to regulate a pololike kinase 1 (PLK1)-dependent pathway at the centrosomes

This article was published online ahead of print in MBoC in Press (http://www.molbiolcell.org/cgi/doi/10.1091/mbc.E17-08-0531) on January 31, 2018.

*Address correspondence to: Christopher A. Maxwell (cmaxwell@bcchr.ubc.ca).

Abbreviations used: bZip, basic leucine zipper motif; HMMR, hyaluronan-mediated motility receptor; Kt-MT, kinetochore–microtubule; MEFs, mouse embryonic fibroblasts; STLC, *S*-trityl-L-cysteine; TPX2, targeting protein for Xklp2.

that locates Ran and modulates nuclear mitotic apparatus (NuMA)-dynein complexes at the cell cortex to correct mispositioned spindles (Connell *et al.*, 2017). Thus, the nonmotor adaptor HMMR may regulate dynein-dependent inward forces on the spindle, but a role, if any, in determining the activity of mitotic kinesins is not yet known.

The activity of kinesins, Eg5 and Kif15, depend on complexes formed with a spindle assembly factor termed targeting protein for Xklp2 (TPX2) (Ma *et al.*, 2011; Drechsler *et al.*, 2014; Balchand *et al.*, 2015; Mann *et al.*, 2017). For example, Eg5 is a homotetramer that can crosslink both antiparallel and parallel microtubules to generate outward-directed forces necessary to organize spindle microtubules (Sawin *et al.*, 1992; Blangy *et al.*, 1995; Kashina *et al.*, 1996; Ma *et al.*, 2011; Gable *et al.*, 2012). Eg5 activity, in turn, is dampened by TPX2: microtubule gliding assays demonstrates that TPX2 imposes steric hindrance on motor stepping (Balchand *et al.*, 2015), and TPX2 restricts Eg5-mediated gliding of antiparallel microtubules and mediates poleward transport of Eg5 along astral microtubules to regulate force generation and focus spindle poles, respectively (Gable *et al.*, 2012). Kif15 can also partner with TPX2 to generate redundant outward-directed force (Wittmann *et al.*, 1998; Tanenbaum *et al.*, 2009). TPX2 localization at microtubule assembly sites, in turn, is reliant on HMMR in both mammalian and *Xenopus* dividing cells (Chen *et al.* 2014; Scrofani *et al.* 2015). Moreover, HMMR and Kif15 share a highly homologous C-terminal, centrosome-targeting, basic leucine zipper motif (bZip) (Wittmann *et al.*, 2000; Maxwell *et al.*, 2003, 2005), which is known to facilitate an interaction with TPX2 (Wittmann *et al.*, 1998; Chen *et al.*, 2014). Therefore, HMMR may influence the Eg5-dependent or Kif15-dependent motor forces that stabilize and organize spindle microtubules and capture, align, and segregate chromosomes.

We recently generated *Hmmr*$^{tm1a/tm1a}$ mice (Connell *et al.*, 2017). Here we isolated *Hmmr*$^{tm1a/tm1a}$ mouse embryonic fibroblasts (MEFs) and identified a delay in metaphase that prevented timely anaphase entry. We modeled this phenotype through the silencing of HMMR in HeLa cells and we identified a requirement for HMMR to facilitate K-fiber stability, enable kinetochore–microtubule (Kt-MT) attachments, and preserve the timely transition from metaphase to anaphase. Using a knockdown-rescue approach, we demonstrate the TPX2-interacting domain in the C-terminus of HMMR contributes to the aforementioned functions. Mechanistically, we demonstrate that HMMR is needed to target TPX2 near to mitotic spindle poles and to promote the formation of TPX2-Eg5 complexes. Proper mitotic progression was restored in HMMR-silenced cells by chemical inhibition of Eg5 but not codepletion of Kif15. We also documented an elevated occurrence of unattached chromosomes in HMMR-silenced HeLa cells, as well as aneuploid genomes in isolated *Hmmr*$^{tm1a/tm1a}$ splenic cells and MEFs. Collectively, our data highlight critical cues provided by the nonmotor adaptor HMMR that balance motor forces and ensure timely entry into anaphase and faithful chromosome segregation.

RESULTS

Progression into anaphase and chromosome segregation are delayed in *Hmmr*$^{tm1a/tm1a}$ cells and HeLa cells treated with HMMR-targeted siRNA

Hmmr$^{tm1a/tm1a}$ mice, in which the *lacZ* gene is inserted after exon 2 in *Hmmr* on both alleles, show neonatal lethality and pleiotropic phenotypes, such as microcephaly and ventricle enlargement, with a corresponding reduction in the mitotic rate of Pax6+ neuroprogenitor cells (Connell *et al.*, 2017). To examine the mitotic process in *Hmmr*$^{tm1a/tm1a}$ cells, we isolated MEFs from *Hmmr*$^{+/+}$ and *Hmmr*$^{tm1a/tm1a}$ E13.5 embryos (Supplemental Figure S1A). The *Hmmr* genotype in MEFs reflected *Hmmr*/HMMR expression levels, as measured with qPCR analysis of mRNA and quantitative Western blot analysis (Supplemental Figure S1, B, and C). When MEFs were followed through cell division with time-lapse imaging, *Hmmr*$^{tm1a/tm1a}$ MEFs required a significantly longer time to complete mitosis (Figure 1, A and B, and Supplemental Movies S1 and S2). Specifically, *Hmmr*$^{tm1a/tm1a}$ MEFs spent longer transitioning from chromosome alignment (metaphase) to segregation (anaphase) (Figure 1, A and C). To model this effect and study the mechanistic function of HMMR for anaphase entry and chromosome segregation, HeLa cells were transfected with either scrambled small interfering RNA (siRNA) or siRNA that targeted the untranslated regions of *HMMR* mRNA, and loss of HMMR expression was confirmed 72 h later (Supplemental Figure S2A). To follow anaphase entry in live cells, asynchronous HeLa cells expressing mCherry-histone H2B were followed with time-lapse imaging (Figure 1D). Multipolar spindles are frequently induced in HMMR-silenced cells (Maxwell *et al.*, 2003), so we focused our analysis on only those metaphase cells with bipolar spindles. To compare the trajectory of metaphase cells, mitotic stages were assigned and color coded every 15 min (Figure 1E). The control cells spent 27 ± 10 min transitioning from chromosome alignment to segregation (Figure 1, E and F, and Supplemental Movie S3). The average duration for this transition was prolonged to 57 ± 26 min in HMMR-silenced cells (Figure 1, E and F, and Supplemental Movie S4) and ~ 55% of HMMR-silenced cells spent >30 min in metaphase prior to anaphase entry. Interestingly, a subset of HMMR-silenced cells (14%) exhibited extensive metaphase arrest (>60 min, orange lines, Figure 1E). In parallel, at 48 h posttransfection, cells were synchronized with a thymidine block and released for 9 h and then mitotic fractions were collected by shake-off every 20 min to analyze the degradation of the mitotic exit inhibitor, cyclin B1 (Supplemental Figure S2B). The intensity of cyclin B1 measured in control cells steadily decreased between 9 and 11 h following release, indicating a progressive entry into anaphase (Supplemental Figure S2C). HMMR-silenced cell populations required significantly longer prior to anaphase entry, as measured through reduction in cyclin B1 intensity (Supplemental Figure S2C). Collectively, these findings suggest HMMR is needed to satisfy the spindle checkpoint and allow timely entry into anaphase.

The spindle checkpoint functions as a rheostat (Collin *et al.*, 2013) and displays a graded response that correlates with the expression levels of key checkpoint proteins, such as BubR1 (Bohers *et al.*, 2008), Mad2 (Niault *et al.*, 2007), and centromere protein A (CENPA) (Amato *et al.*, 2009). To test whether delayed anaphase entry in HMMR-silenced cells corresponded with increased expression of these proteins, we examined the abundance of key checkpoint proteins in synchronized cells. The expression of BubR1, NDC80, Aurora B, and Mad2 was comparable in lysates obtained from control-treated or HMMR-silenced mitotic cells (Supplemental Figure S3A). Also, the localization of these proteins was unaffected: BubR1 located to individual kinetochore as discrete puncta (Supplemental Figure S3B), Aurora B localized throughout chromosome arms (Supplemental Figure S3C), and Mad2 only located to unattached kinetochores (Supplemental Figure S3D). These findings suggest that HMMR is dispensable for the expression and abundance of key checkpoint proteins.

HMMR promotes microtubule–kinetochore attachments and interkinetochore tension

Chromosome segregation is initiated with bipolar attachment of all chromosomes to the spindle. The number of inappropriate chromosome attachments, as measured by Mad2-positive kinetochores

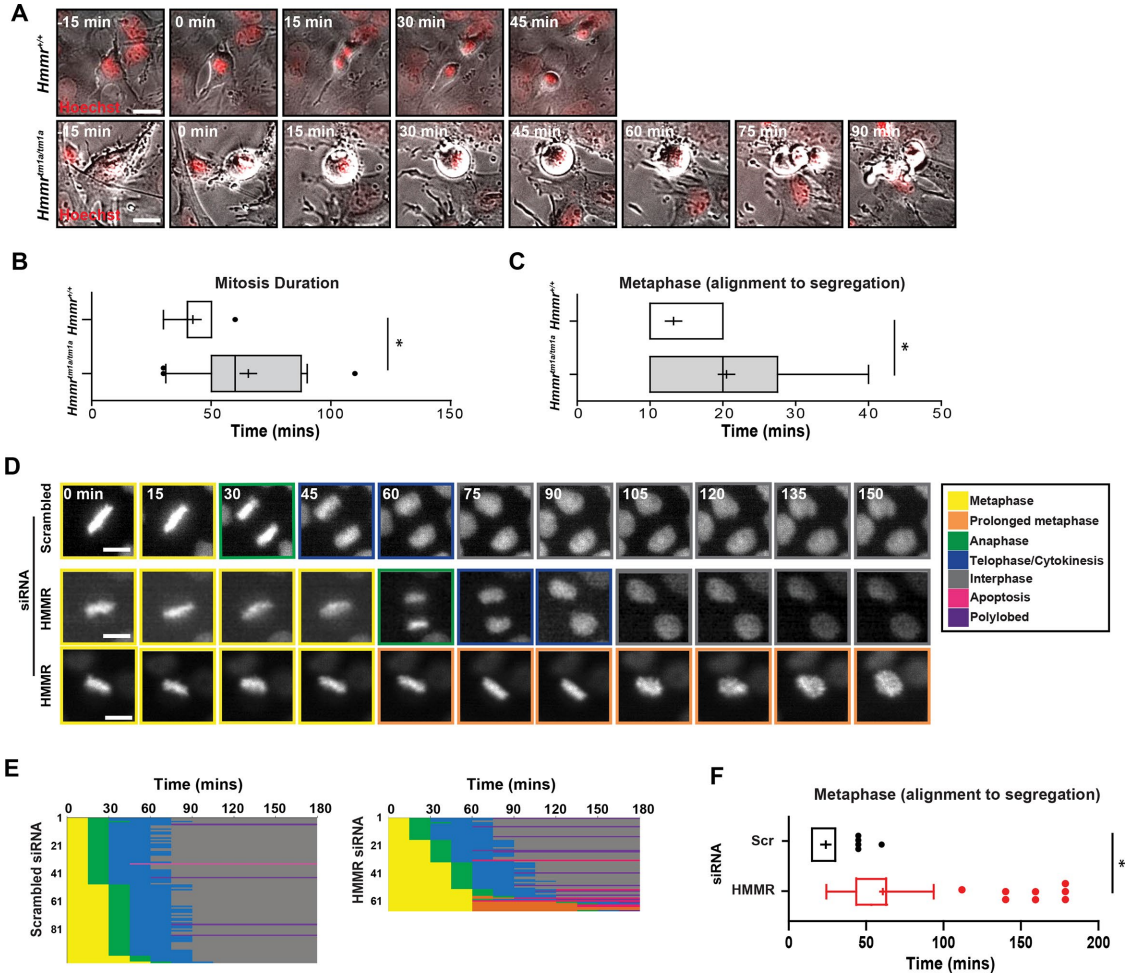

FIGURE 1: HMMR is required for timely segregation of chromosomes in HeLa cells and MEFs derived from *Hmmr*$^{tm1a/tm1a}$ animals. (A) MEFs collected from *Hmmr*$^{+/+}$ and *Hmmr*$^{tm1a/tm1a}$ littermates were labeled with Hoechst to visualize DNA during time-lapse microscopy. 0 min marks the start of mitosis. Scale bars = 10 μm. (B) Quantification of mitosis duration in *Hmmr*$^{+/+}$ and *Hmmr*$^{tm1a/tm1a}$ MEFs. (box-and-whisker plots display the median flanked by the 10th, 25th, 75th, and 90th percentiles, and the + sign marks the mean; $N = 4$; >25 cells/bar; *$p < 0.0001$, *t* test). (C) Quantification of transition time from metaphase to anaphase in *Hmmr*$^{+/+}$ and *Hmmr*$^{tm1a/tm1a}$ MEFs (box-and-whisker plots display the median flanked by the 10th, 25th, 75th, and 90th percentiles, and the + sign marks the mean; $N = 4$; >25 cells/bar; *$p < 0.0001$, *t* test). (D) Representative time-lapse images of mitotic HeLa cells expressing mCherry Histone-H2B after siRNA treatment. 0 min marks the start of metaphase. Scale bars = 10 μm. (E) The kinetics of metaphase to anaphase transition, mitotic exit, and daughter cell morphology from time-lapse images of HeLa cells expressing mCherry Histone-H2B after siRNA treatment. 0 min marks the start of metaphase. (F) Quantification of transition time from metaphase to anaphase measured from 1E (box-and-whisker plots display the median flanked by the 10th, 25th, 75th, and 90th percentiles, and the + sign marks the mean; $N = 4$; >65 cells/bar; *$p < 0.0001$, *t* test).

in each cell, was increased in HMMR-silenced cells (Figure 2A). We also compared interkinetochore distances in control-treated and HMMR-silenced cells to confirm the presence of inappropriate chromosome attachments and measure tension generated between sister kinetochores on bipolar attachment (McIntosh, 1991; Li and Nicklas, 1997). Previous investigations demonstrated that metaphase spindles may be mispositioned or tilted following loss of HMMR expression in human and murine cells (Dunsch *et al.*, 2012; Li *et al.*, 2016; Connell *et al.*, 2017). A tilted spindle will distort distances (both spindle length and interkinetochore distance) viewed along the *z*-axis (Supplemental Figure S4A), and spindles poles were frequently found on different *z*-axis slices in HMMR-silenced cells (Supplemental Figure S4B). Thus, to accurately measure interkinetochore distance, we measured the distance between NDC80 foci along a plane that is perpendicular to the aligned chromosomes in a rotated three-dimensional (3D) image, using tubulin gamma-1 (TUBG1) as a marker for spindle poles (Supplemental Figure S4B). Measurements collected from a rotated view of the spindle showed decreased interkinetochore distance in HMMR-silenced cells (Supplemental Figure S4C), which was comparable to cells treated with 3.5 nM vincristine, a microtubule destabilizing drug (Figure 2B). Finally, we incubated cells at 4°C for 20 min to disassemble nonkinetochore microtubules and test the stability of kinetochore fibers (K-fibers), which are the main type of spindle microtubules needed to form stable Kt-MT attachments. While numerous K-fibers were detected in control-treated cells, HMMR-silenced cells contained few cold-stable K-fibers (Figure 2C). These findings indicate that HMMR is needed to promote Kt-MT attachments, interkinetochore tension, and K-fiber stability needed for anaphase entry.

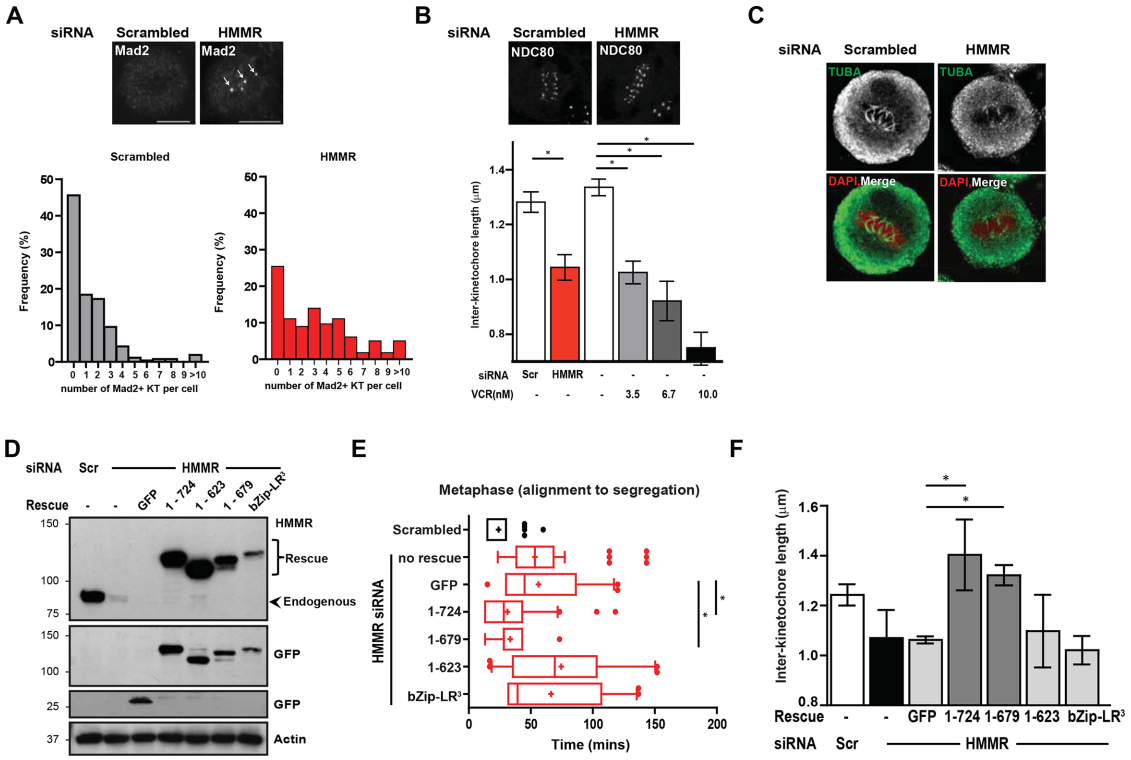

FIGURE 2: The C-terminal bZip motif in HMMR is required for proper metaphase to anaphase transition and interkinetochore tension. (A) Histogram of Mad2-positive kinetochores per cell in HeLa cells treated with control or HMMR-targeting siRNA. Only cells with bipolar spindles were analyzed ($N = 4$; >200 cells/treatment). Scale bars = 10 μm. (B) Interkinetochore distance was measured based on NDC80 staining in HeLa cells treated with control or HMMR-targeted siRNA (as described in Supplemental Figure S4) or vincristine (diluted in water). Only cells with bipolar metaphase spindles were analyzed. Analysis of ≥70 kinetochores from 80 cells per treatment (mean ± SD; $N = 4$; *$p < 0.001$ for all comparisons, ANOVA). Scale bars = 10 μm. (C) HeLa cells treated with control or HMMR-targeted siRNA were incubated in 4°C for 20 min prior to fixation and stained for TUBA to visualize cold-stable microtubules. Scale bars = 10 μm. Representative images of $N = 3$. (D) Western blot analysis confirmed the expression of GFP-HMMR constructs in HeLa cells depleted of endogenous HMMR by siRNA. Actin served as the loading control. Representative Western blot analysis from $N = 2$ experiments. (E) Quantification of the transition time from metaphase to anaphase for HMMR-silenced cells transfected with GFP-HMMR variants (box-and-whisker plots display the median flanked by the 10th, 25th, 75th, and 90th percentiles, and the + sign marks the mean; $N = 3$; >30 cells/bar; **$p = 0.0021$ for 1–724 and $p = 0.0074$ for 1–679 compared with GFP, ANOVA). (F) Interkinetochore tension was measured in bipolar metaphase spindles based on NDC80 staining (as described in Supplemental Figure S4) in cells treated as indicated. Analysis of 35 cells per treatment (mean ± SD; $N = 3$; *$p = 0.0095$ for 1–724 and $p = 0.0314$ for 1–679 compared with GFP, ANOVA).

To determine the functional domains in HMMR needed to promote anaphase entry, we transiently introduced siRNA-resistant green fluorescent protein (GFP)-HMMR truncation constructs into HMMR-silenced cells. We determined 48 h posttransfection to be the optimal time for GFP-HMMR expression (Figure 2D) and then performed time-lapse microscopy during this time frame. With respect to GFP expression alone, expression of GFP-HMMR constructs that contained the bZip motif (full-length:1–724, and 1–679) promoted timely entry into anaphase (Figure 2E). Expression of either GFP-HMMR$^{1\text{-}623}$, which lacks the bZip motif, or a construct where three conserved leucines were mutated to arginines, GFP-HMMR (bZip-LR^3), did not alter the kinetics for anaphase entry. We performed parallel rescue experiments in *Hmmr*$^{tm1a/tm1a}$ MEFs and observed similar kinetics (Supplemental Figure S5, A–C). Next, we examined interkinetochore distance in fixed HeLa cells. Again, the expression of GFP-HMMR constructs that contained the bZip motif restored tension across sister kinetochores in HMMR-silenced cells (Figure 2F). These rescue experiments reveal that timely entry into anaphase requires the bZip motif in HMMR, which is known to interact with TPX2 (Chen *et al.*, 2014) and is homologous with a domain in Kif15 (Maxwell *et al.*, 2003).

HMMR attenuates Eg5 activity by promoting Eg5–TPX2 complex formation

The bZip motif in HMMR promotes an interaction between TPX2 and Aurora A, which stimulates kinase activity and microtubule nucleation (Joukov *et al.*, 2006; Chen *et al.*, 2014; Scrofani *et al.*, 2015). As TPX2 interacts with kinesin motors to modulate K-fiber stability (Ma *et al.*, 2010, 2011), we performed a series of coimmunoprecipitation experiments to determine whether these interactions are altered in HMMR-silenced cells. We optimized our procedures to obtain high-efficiency immunoprecipitation of the targeted proteins (Supplemental Figure S6A) and, in control-treated cell lysates, to coimmunoprecipitate known interactors, including TPX2 with Eg5, Kif15, and HMMR (Supplemental Figure S6B). In separate immunoprecipitation experiments using control-treated lysates, we noted that antibodies raised against either the N-terminus or the C-terminus of HMMR coprecipitated TPX2 and Kif15 but not Eg5 or NuMA (Figure 3A).

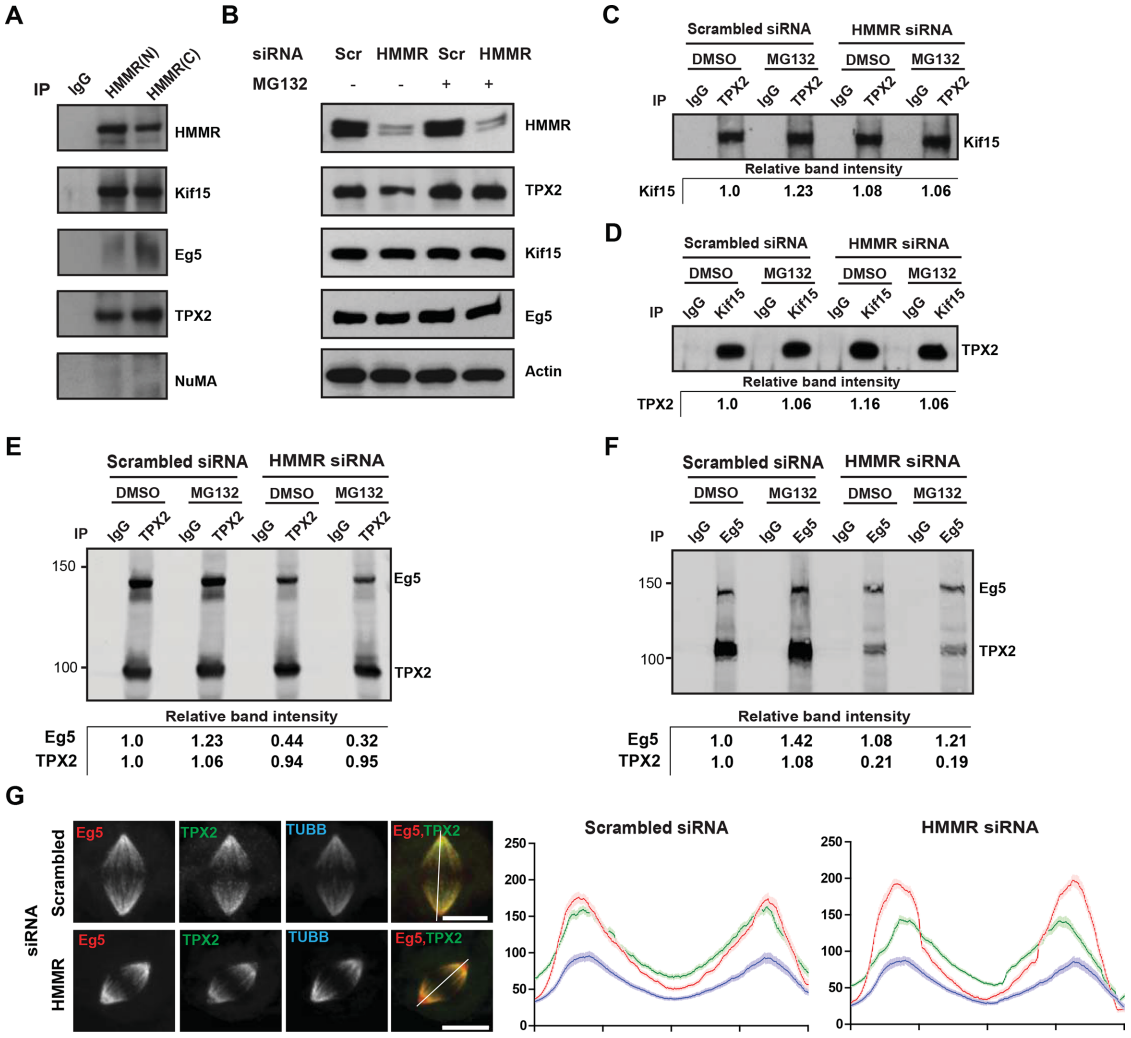

FIGURE 3: HMMR silencing attenuates TPX2-Eg5 interaction due to mislocalization of TPX2. (A) HeLa cells were synchronized to early mitosis, lysed, and precipitated with immunoglobulin G (IgG) or antibodies recognizing either the N- or C-terminus of HMMR. Immunoprecipitated proteins were identified by Western blot analysis using the indicated antibodies targeting Kif15 or Eg5. Antibodies targeting TPX2 or those targeting NuMA were included as positive or negative controls. Representative Western blot analysis from $N = 4$ experiments. (B) Control-treated or HMMR-silenced HeLa cells were synchronized to early mitosis. Prior to lysis, cells were treated with MG132 or DMSO. Protein abundance was determined by Western blot analysis. Actin served as the loading control. Representative Western blot analysis from $N = 4$ experiments. (C) Control-treated or HMMR-silenced HeLa cells were synchronized to early mitosis. Prior to lysis, cells were treated with MG132 or DMSO. Cell lysates were precipitated with IgG or antibodies recognizing TPX2 and Western blot analysis of Kif15 revealed similar levels in control-treated and HMMR-silenced cells. Representative Western blot analysis from $N = 4$ experiments. (D) Control-treated or HMMR-silenced HeLa cells were synchronized to early mitosis. Prior to lysis, cells were treated with MG132 or DMSO. Cell lysates were precipitated with IgG or antibodies recognizing Kif15, and Western blot analysis of TPX2 revealed similar levels in control-treated and HMMR-silenced cells. Representative Western blot analysis from $N = 4$ experiments. (E) Control-treated or HMMR-silenced HeLa cells were synchronized to early mitosis. Prior to lysis, cells were treated with MG132 or DMSO. Cell lysates were precipitated with IgG or antibodies recognizing TPX2. Quantitative Western blot analysis revealed similar levels of TPX2 in lysates generated from control-treated and HMMR-silenced cells but reduced levels of coprecipitated Eg5 in lysates generated from HMMR-silenced cells. Protein bands were visualized using IR fluorophore-tagged secondary antibodies. Representative Western blot analysis from $N = 4$ experiments. (F) Control-treated or HMMR-silenced HeLa cells were synchronized to early mitosis. Prior to lysis, cells were treated with MG132 or DMSO. Cell lysates were precipitated with IgG or antibodies recognizing Eg5. Quantitative Western blot analysis revealed similar levels of Eg5 in lysates generated from control-treated and HMMR-silenced cells but reduced levels of coprecipitated TPX2 in lysates generated from HMMR-silenced cells. Protein bands were visualized using IR fluorophore-tagged secondary antibodies. Representative Western blot analysis from $N = 4$ experiments. (G) Maximum intensity projection of immunofluorescence analysis for TPX2, Eg5, and TUBB localization in control-treated or HMMR-silenced cells. Scale bars = 10 μm. Line scan analysis of fluorescence intensity profiles are provided for metaphase spindles in control-treated or HMMR-silenced cells (mean ± SD; $N = 2$, 30 cells/treatment).

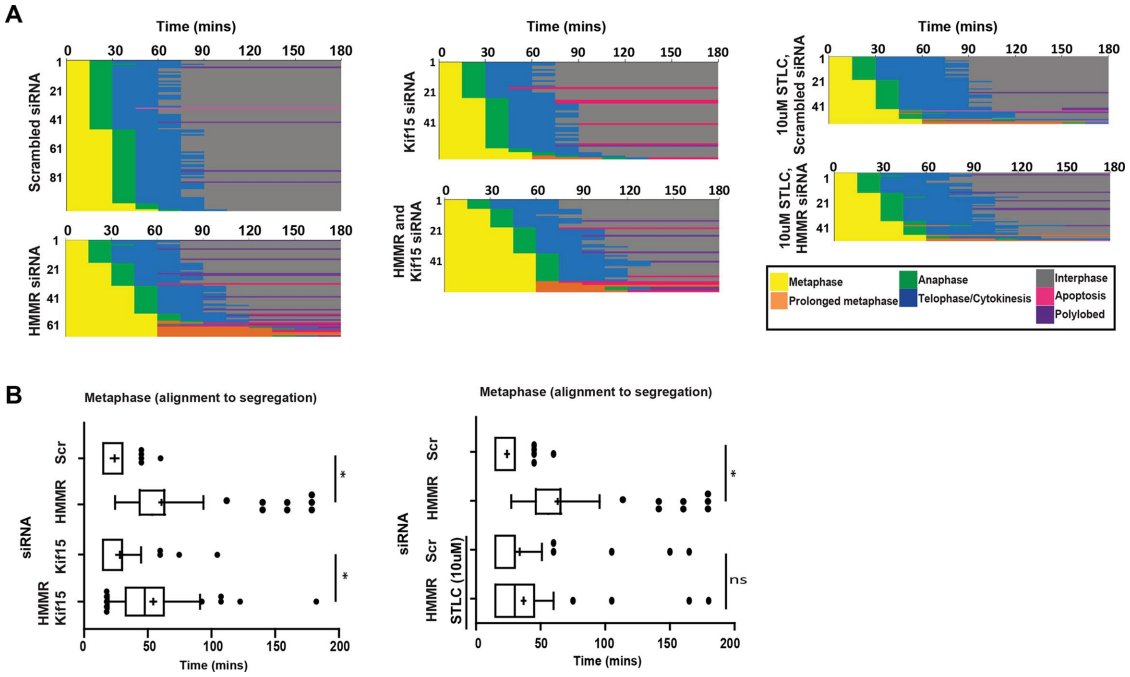

FIGURE 4: Eg5 inhibition is sufficient to rescue aberrant checkpoint kinetics in HMMR-silenced cells. (A) The kinetics of metaphase to anaphase transition, mitotic exit, and daughter cell morphology as extracted from time-lapse images of HeLa cells expressing mCherry Histone-H2B after indicated siRNA treatment and/or treatment with the Eg5 inhibitor STLC. 0 min marks the start of metaphase. (B) Quantitation of transition time from metaphase to anaphase in control-treated or HMMR-silenced cells codepleted of Kif15 (left-hand side) or treated with the Eg5 inhibitor STLC (right-hand side) (box-and-whisker plots display the median flanked by the 10th, 25th, 75th, and 90th percentiles, and the + sign marks the mean; $N = 3$; >40 cells/bar; *$p < 0.0001$, *t* test).

The abundance of TPX2 is reduced in HMMR-silenced cell lysates and can be restored through proteasome inhibition with MG132 (Figure 3B), as previously reported (Chen *et al.*, 2014; Scrofani *et al.*, 2015). Thus, for subsequent immunoprecipitation experiments, cells were pretreated with MG132, or vehicle control, prior to lysis to ensure that the levels of TPX2 were comparable in control-treated and HMMR-silenced cell lysates (Figure 3B). Having established the presence of endogenous TPX2-Eg5 and TPX2-Kif15 complexes, we queried whether the TPX2-Kif15 complex is altered in HMMR-silenced cells. The abundance of Kif15 (Figure 3B) and the reciprocal coprecipitation of TPX2-Kif15 complexes were not distinguishable between control-treated and HMMR-silenced cell lysates (Figure 3, C and D), indicating that HMMR is dispensable for the formation of TPX2-Kif15 complexes. We next tested whether the loss of HMMR may indirectly affect Eg5-TPX2 complex formation. We utilized secondary antibodies conjugated with near-infrared fluorescent dyes to detect the levels of coprecipitated proteins (TPX2 or Eg5) in the same gel in a quantitative manner (Figure 3, E and F). Following precipitation with TPX2 antibodies, we observed a quantitative loss of coprecipitated Eg5 levels in HMMR-silenced cell lysates (Figure 3E). Conversely, we observed a quantitative loss of TPX2 coprecipitated with Eg5 antibodies from HMMR-silenced cell lysates (Figure 3F). We then examined TPX2, Eg5, and tubulin beta (TUBB) fluorescence intensities along the mitotic spindle with line scan analysis in control-treated and HMMR-silenced cells. In control-treated cells, the intensity projections for Eg5, TPX2, and TUBB overlapped along spindle microtubules with maximum intensities at spindle poles, as indicated by the TUBB intensity (Figure 3G). In HMMR-silenced metaphase cells, however, the peak intensity for TPX2 was shifted slightly away from the Eg5 peak intensity at spindle poles (Figure 3G). Together, these data indicate that HMMR is needed to promote TPX2-Eg5 complex formation and to localize TPX2 near spindle poles.

Hyperactive Eg5 activity delays anaphase entry in HMMR-silenced cells

Each of the phenotypes we observed in HMMR-silenced cells (e.g., delayed anaphase entry, loss of cold-stable K-fibers, and increased Mad2-positive kinetochores) is similar to those that result from the excess outward forces that follow the loss of dynein activity (van Heesbeen *et al.*, 2014). The reduced formation of inhibitory Eg5-TPX2 complexes observed in HMMR-silenced cells would be predicted to result in increased net outward force and putative imbalance within the spindle. Therefore, we predicted that the inhibition of kinesin activity may restore timely anaphase entry in HMMR-silenced metaphase cells. To test this prediction, we treated HMMR-silenced or scrambled siRNA-treated cells with one of two small-molecule inhibitors of Eg5, *S*-trityl-L-cysteine (STLC) or monastral or codepleted Kif15 by pretreatment with siRNA. We efficiently silenced HMMR and/or Kif15 (Supplemental Figure S7A) prior to time-lapse imaging of mitotic HeLa cells expressing mCherry-H2B (Supplemental Figure S7B). For each of these treatments, we analyzed the progression of metaphase cells that had achieved chromosome alignment with phenotypically normal bipolar spindles. Neither Eg5 inhibition nor Kif15 depletion alone significantly altered the kinetics of anaphase entry for selected metaphase cells with bipolar spindles (Figure 4, A and B). In HMMR-silenced cells, cotreatment with either STLC (Figure 4, A and B, and Supplemental Figure S8, A–C) or monastral (Supplemental Figure S8, A–C) but not codepletion of Kif15 (Figure 4, A and B), was sufficient to recover timely entry into anaphase. Next, we quantified spindle morphology following Eg5 inhibition in HMMR-silenced cells (Supplemental Figure

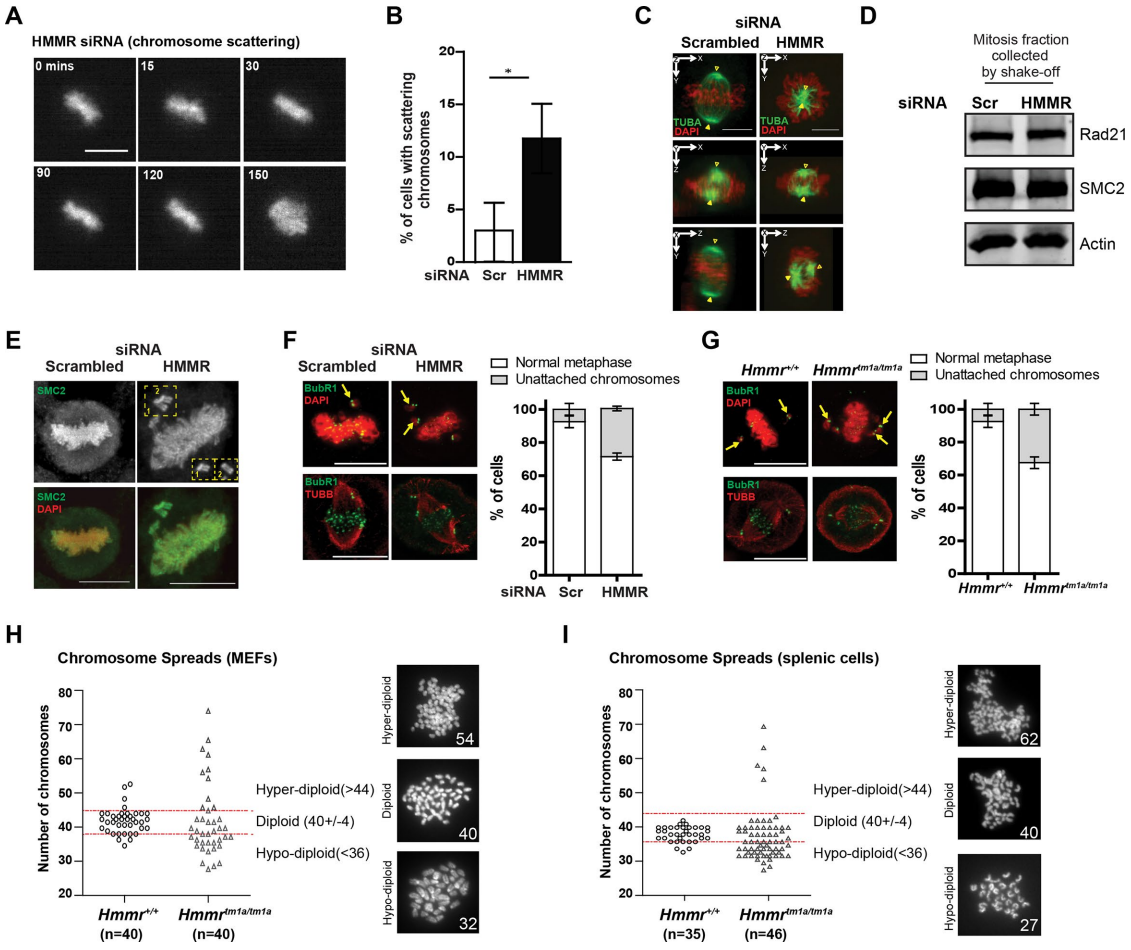

FIGURE 5: *Hmmr*$^{tm1a/tm1a}$ cells display genome instability as a result of chromosome attachment errors. (A) A chromosome scattering phenotype accompanies the prolonged metaphase delay observed in HMMR-silenced HeLa cells expressing mCherry Histone-H2B. 0 min marks the start of metaphase. Scale bars = 10 μm. (B) The frequency of chromosome scattering phenotype (shown in A) in control-treated or HMMR-silenced cells (mean ± SD; $N = 4$; >65 cells/bar; *$p < 0.0001$, *t* test). (C) HMMR-silenced metaphase cells with rotated spindles appear to display scattered chromosomes. Maximum intensity projections (*z*-axis) of cells are shown in the top row. The full 3D z-projections are rotated to view the spindle from various planes. Arrow heads indicate individual spindle pole. Scale bars = 10 μm. (D) Control-treated or HMMR-silenced HeLa cells were synchronized to early mitosis, collected by shake-off method, and lysed. Quantitative Western blot analysis of cell lysates did not reveal a difference in the expression of components of the cohesin complex. Actin served as the loading control. Representative Western blot analysis from $N = 4$ experiments. (E) HeLa cells (treated as indicated) were synchronized to early mitosis and stained for SMC2. Maximum intensity projections of the chromosomal mass show two stray SMC-positive chromosomes in the HMMR-silenced metaphase cell. These chromosomes are boxed and shown individually in the inlay ($n = 3$). (F) Quantification of the proportion of metaphase cells with unattached chromosomes based on BubR1 immunofluorescence (marked by arrows) in control-treated or HMMR-silenced HeLa cells (mean ± SD; $N = 2$; >80 cells/bar). Scale bars = 10 μm. (G) Quantification of the proportion of metaphase cells with unattached chromosomes based on BubR1 immunofluorescence (marked by arrows) in *Hmmr*$^{+/+}$ and *Hmmr*$^{tm1a/tm1a}$ MEFs (mean ± SD; $N = 2$; >40 cells/bar). Scale bars = 10 μm. (H) Chromosome spreads of MEFs collected from *Hmmr*$^{+/+}$ and *Hmmr*$^{tm1a/tm1a}$ littermates. Cells with 40 ± 4 chromosomes were classified as a diploid phenotype. (I) Chromosome spreads of splenic cells collected from *Hmmr*$^{+/+}$ and *Hmmr*$^{tm1a/tm1a}$ littermates. Cells with 40 ± 4 chromosomes were classified as a diploid phenotype.

S9A). We noted an increase in the proportion of metaphase cells with bent and buckled microtubules, similar to those resulting from the expression of a dominant negative truncated TPX2 mutant that lacked the Eg5 binding domain (Ma *et al.*, 2010, 2011), and Eg5 inhibition reduced the frequency of these abnormal metaphase spindles (Supplemental Figure S9A). Moreover, in fixed HMMR-silenced cells, 10 μM STLC treatment was sufficient to reduce the number of Mad2-positive cells (Supplemental Figure S9B) and to restore interkinetochore tension (Supplemental Figure S9C) and cold-stable K-fibers (Supplemental Figure S9D). However, Eg5 inhibition did not reduce the frequency of mispositioned spindles in HMMR-silenced cells (Supplemental Figure S9A). Thus, dampening Eg5-mediated outward forces promotes bipolar chromosome attachment, interkinetochore tension, and anaphase entry in HMMR-silenced cells.

Hmmr$^{tm1a/tm1a}$ cells display genome instability

A subset of HMMR-silenced metaphase cells displayed an apparent chromosome scattering phenotype during the delayed transition from metaphase to anaphase (Figure 5, A and B). On close inspection, however, it was clear that HMMR-silenced cells with scattered

chromosomes were undergoing spindle rotation (Supplemental Movies S5 and S6). Typically, when the mitotic spindle is positioned parallel to the growth surface, the chromosomal mass appears as a barlike array (Figure 5C, top left). However, metaphase spindles often rotated in HMMR-silenced cells (Connell *et al.*, 2017), and as the spindle approached a position perpendicular to the growth surface, the chromosome mass would appear scattered (Figure 5, B and C, top right). Both chromosome scattering and spindle rotation are associated with cohesion fatigue, which leads to asynchronous separation of chromatids through loss of the cohesin complex (Daum *et al.*, 2012; Gorbsky, 2013). In HMMR-silenced cells, however, we observed no alterations to components of the cohesin complex: the abundance of Rad21 and SMC2 (Figure 5D) and the localization of SMC2 along the entire chromosome volume was not affected in HMMR-silenced cells (Figure 5E). Also, HMMR-silenced cells displayed stray or unattached chromosomes (Figure 5E, inset), which are not consistent with the stray chromatids that often accompany cohesion fatigue. In fact, immunofluorescence detection of the kinetochore marker BubR1 indicated the presence of unattached chromosomes in 28% of HMMR-silenced metaphase cells, which was significantly higher than in control-treated cells (Figure 5F). When we performed the same analysis in *Hmmr*$^{+/+}$ or *Hmmr*$^{tm1a/tm1a}$ MEFs, we noted a similar increase in the proportion of metaphase cells with unattached chromosomes (Figure 5G) and a significant proportion of *Hmmr*$^{tm1a/tm1a}$ MEFs produced aneuploid chromosome spreads, where diploid was defined as 40 ± 4 chromosomes (Figure 5H). We then isolated splenic cells from 3-mo-old *Hmmr*$^{+/+}$ and *Hmmr*$^{tm1a/tm1a}$ animals for overnight culture and chromosome analysis. While the majority of chromosome spreads obtained from *Hmmr*$^{+/+}$ splenocytes were diploid, we observed similar increases in the frequency of aneuploid spreads from *Hmmr*$^{tm1a/tm1a}$ splenocytes (Figure 5I). These data indicate a critical role for HMMR in the maintenance of chromosome segregation and genome integrity.

DISCUSSION

HMMR is a nonmotor adaptor protein involved in mitotic spindle assembly (Manning and Compton, 2008). Nonmotor adaptor proteins help to equilibrate motor force activities that organize the metaphase spindle and capture, align, and segregate chromosomes. To date, there are limited studies reporting the functional importance of these adaptors on force balance and anaphase entry. By examining primary cells with genetic deletion of HMMR or by silencing HMMR in immortalized HeLa cells and following the resultant mitotic phenotypes, we demonstrate that this nonmotor adaptor protein is needed to organize spindle microtubules, stabilize K-fibers, facilitate Kt-MT attachments, and generate interkinetochore tension to ensure timely anaphase entry and faithful chromosome segregation.

The mitotic phenotypes observed in HMMR-silenced cells are consistent with a net gain of outward force applied to the bipolar spindle. Indeed, in HMMR-silenced cells, we noted a reduction in the formation of inhibitory TPX2-Eg5 complexes that are known to dampen Eg5 activity, as well as disturbed colocalization between TPX2 and Eg5 near spindle poles. These findings complement recent reports that HMMR regulates TPX2 localization in nonmitotic cells (Chu *et al.*, 2018) and at prophase centrosomes (Eibes *et al.*, 2018). Eg5 is known to be transported to microtubule minus ends through dynein (Uteng *et al.*, 2008; Gable *et al.*, 2012), and we find that HMMR is dispensable to Eg5 localization at these sites. However, TPX2 is less abundant at spindle poles in HMMR-silenced cells and thus may be less available to complex with Eg5 at these sites, which has also been postulated to occur at prophase centrosomes dependent on NEK9 phosphorylation of TPX2 (Eibes *et al.*, 2018). In a similar manner, HMMR promotes complex formation between TPX2 and Aurora A during spindle assembly (Chen *et al.* 2014; Scrofani *et al.*, 2015).

While the inhibition of Eg5 activity was sufficient to rescue mitotic kinetics in HMMR-silenced cells, we found that Kif15 depletion was ineffective. HMMR and Kif15 share a similar C-terminal bZip motif, but HMMR likely does not compete with Kif15 to bind TPX2, as we did not detect any changes to Kif15-TPX2 complex formation in HMMR-silenced cells. Kif15 motor stepping is inhibited by TPX2 in vitro (Tanenbaum *et al.*, 2009; Drechsler *et al.*, 2014; Mann *et al.*, 2017), but Kif15 may be less susceptible than Eg5 to TPX2 inhibition due to structural differences between the motors (Mann *et al.*, 2017). Indeed, the principal mechanism for Kif15 inhibition was reported to be self-repression through its C-terminal Coil-2 region (Sturgill *et al.*, 2014). Therefore, the impaired localization of TPX2 near spindle poles in HMMR-silenced cells is sufficient to alter the regulation of Eg5 but not Kif15 motor activity.

Our findings in HMMR-silenced cells indicate Eg5 activity is less restricted but do not exclude the possibility that dynein-dependent inward forces are also reduced. However, the abundance of checkpoint complexes at the kinetochore, which would be expected to be increased in an environment with reduced dynein-dependent stripping activity (Howell *et al.*, 2001; Wojcik *et al.*, 2001), were unchanged in HMMR-silenced cells. We attribute the retention of Mad2 on kinetochores in HMMR-silenced cells to a deficit in stable K-fibers. Unrestricted Eg5 activity or movement may prevent sufficient cross-linking between microtubules emanating out of the centrosomes and K-fibers. As a consequence, K-fibers would be less stable and not properly incorporated into the rest of the spindle microtubule matrix, which would delay the accumulation of stable attachments and reduce tension. Similar loss of K-fiber stability and reduced interkinetochore tension phenotypes were associated with the expression of a dominant negative truncated TPX2 mutant that lacked the Eg5 binding domain (Ma *et al.*, 2010).

In both mammalian and *Xenopus* dividing cells, HMMR is not essential for K-fiber assembly (Groen *et al.*, 2004; Chen *et al.*, 2014; Scrofani *et al.*, 2015), suggesting that the initial nucleation of K-fibers is not defective in HMMR-silenced cells. However, bent or buckled microtubules were more frequently observed in HMMR-silenced cells, which may reduce the probability that the NDC80 complex at the kinetochore binds these microtubules to facilitate chromosome attachment (Ciferri *et al.*, 2008; Wang *et al.*, 2008; Alushin *et al.*, 2010). Alternatively, HMMR may be needed to stabilize Kt-MT attachments directly via the NDC80 complex. A putative HMMR and NDC80 interaction was identified in an immunoprecipitation/mass spectometry (IP/MS) mitotic screen (Neumann *et al.*, 2010), although the mechanistic details behind this interaction has not been investigated. Finally, it is possible that HMMR is needed to promote the correction of improperly attached chromosomes through Aurora A. HMMR is known to promote Aurora A activity in both mammalian and *Xenopus* cells (Chen *et al.*, 2014; Scrofani *et al.*, 2015). A gradient of Aurora A activity at spindle poles was implicated in the correction of improperly attached chromosomes through the selective disassembly of K-fibers (Chmátal *et al.*, 2015; Ye *et al.*, 2015). This attachment error correction is reliant on two Aurora A substrates, CENP-A (Kunitoku *et al.*, 2003) and NDC80 (Ye *et al.*, 2015). Thus, defective Kt-MT attachments that occur in HMMR-silenced cells may result from elevated Eg5 activity and a defective error correction mechanism due to reduced Aurora A activity.

In addition to defects in Kt-MT attachments and delayed anaphase entry, HMMR-silenced cells were prone to undergo spindle rotation and display scattered chromosome phenotypes and

unattached chromosomes. One potential mechanistic explanation is that HMMR-silenced cells that underwent prolonged delay during metaphase were subjected to cohesion fatigue; however, a number of observations in HMMR-silenced cells do not support this putative mechanism: components of the cohesion complex appeared unaffected, and unattached chromosomes, rather than precocious sister chromatid separation, were observed. Unattached chromosomes could lead to chromosome segregation errors and the induction of genome instability, and we saw frequent aneuploid chromosome spreads in cells (both MEFs and splenic cells) isolated from *Hmmr*$^{tm1a/tm1a}$ animals (Connell *et al.*, 2017). An induction of aneuploid progeny in cells lacking HMMR may help explain the genetic linkage between elevated risk to develop breast cancer and variation in the *HMMR* locus that results in reduced gene product (Pujana *et al.*, 2007; Maxwell *et al.*, 2011). Moreover, the production of aneuploid neuroprogenitor cells associates with microcephaly (Marthiens *et al.*, 2013), which is also observed in *Hmmr*$^{tm1a/tm1a}$ animals but was attributed to misoriented neuroprogenitor cell divisions (Connell *et al.*, 2017).

Taken together, our data are consistent with a model wherein HMMR, via the bZip motif, locates TPX2 near microtubule minus ends, which enables TPX2-Eg5 complex formation. HMMR-mediated regulation of Eg5 activity is needed to stabilize the bipolar spindle and promote kinetochore–microtubule attachments that are necessary for timely anaphase entry and faithful chromosome segregation (Supplemental Figure S10). These data highlight the importance of a nonmotor adaptor protein in the modulation of motor activities and the maintenance of genome stability.

MATERIALS AND METHODS

Cell culture

HeLa cells were cultured in DMEM (Thermo-Fisher) supplemented with 10% fetal bovine serum (FBS; Invitrogen), 20 U/ml penicillin (Invitrogen), and 20 µg/ml streptomycin (Invitrogen). HeLa cells that stably express eGFP-tubulin alpha (TUBA) and mCherry-Histone-H2B were maintained with 0.3 µg/ml puromycin (Invitrogen) and 0.5 µg/ml blasticidin S (Invitrogen). Cells were synchronized by a double thymidine block with 2 mM thymidine (Sigma) (Chen *et al.*, 2014).

Reagents and antibodies

Proteasome inhibitor MG132 (Sigma), Monastrol (Sigma), and STLC (Tocris Bioscience) were used as indicated. The following antibodies were used: β-actin (Sigma), Aurora kinase B (Cell Signaling), BubR1 (Cell Signaling), CENPA (Abcam), Cyclin B1 (Abcam), Eg5 (Abcam), GFP (Abcam), HMMR (Abcam), Kif15 (Abcam), NDC80 (Abcam), NuMA (Cell Signaling), Mad2 (Millipore), HMMR (Abcam), TPX2 (Novus Biologicals), TUBA (Abcam), and TUBG1 (Sigma). Secondary antibodies were conjugated to infrared dye (IRDye) (Rockland), horseradish peroxidase (HRP) (Sigma), or to Alexa Fluor 488, 594, or 647 (Invitrogen). 4′,6-Diamidino-2-phenylindole (DAPI) was purchased from Sigma Aldrich.

Immunoprecipitation and Western blot analysis

Mitotic cells were collected by shaking at high speed and then centrifuged. Cells were lysed in radioimmunoprecipitation assay (RIPA) buffer (Western blot) or immunoprecipitation buffer (50 mM Tris-HCl, pH 7.4, 150 mM NaCl, 1 mM EDTA, 0.5% NP-40) supplemented with protease and phosphatase inhibitors (Roche). Cell lysates were clarified by centrifugation, and protein concentration was determined using the bicinchoninic acid (BCA) protein assay kit (Pierce). For immunoprecipitation, lysates were precleared with protein G or A/G PLUS-Agarose beads (Santa Cruz). Protein complexes were isolated by incubation indicated antibodies for at 4°C overnight on rotation and then with protein G or A/G PLUS-Agarose beads for 6 h at 4°C on rotation. Isolated complexes were washed four times and then mixed with SDS sample buffer, separated by SDS–PAGE, and blotted with indicated primary antibodies and detected by HRP- or IRDye-conjugated antibodies and enhanced chemiluminescence (GE Healthcare) or the Odyssey infrared (IR) imaging (LI-COR) system, respectively.

Immunofluorescence and image acquisition

Cells grown on coverslips were fixed with cold methanol and then permeabilized with phosphate-buffered saline (PBS)-0.25% Triton X-100 and blocked with 2% bovine serum albumin (BSA) in PBS for 1 h. Antibodies were diluted in PBS with 0.1% Triton X-100 and 3% BSA. Coverslips were mounted with ProLong Gold Antifade Reagent containing DAPI (Invitrogen).

Fixed cells were imaged using a 60× 1.2 NA oil objective with Fluoview software (Olympus) on an Olympus Fluoview FV10i confocal microscope (Olympus). Maximum intensity projection of each fluorescence channel was performed in ImageJ v1.46j (National Institutes of Health).

For live-cell imaging, cells were grown in 96-well plates (Corning) and imaged using a 40× 0.75 NA dry objective with MetaXpress 5.0.2.0 software (Molecular Devices) on an ImageXpress Micro XL epifluorescence microscope (Molecular Devices). Images were taken every 15 min, and movies were made in MetaXpress 5.0.2.0 software (Molecular Devices).

Genotyping

Ear notches were lysed in buffer (100 mM Tris, pH 8.8, 100 mM $[NH_4]_2SO_4$, 100 mM $MgCl_2$, 1% β-mercaptoethanol, 0.5% Triton X-100, and 1.6 mg/ml protease K) at 50°C for 3–5 h. PCR was performed using AccuStart II PCR mix (Quanta Biosciences). Primers used as described in Connell *et al.* (2017).

Quantitative PCR of mRNA levels in MEFs

Quantitative PCR conditions were as previously described (Chen *et al.*, 2014). Analysis of results was done using the ΔΔCt method and normalized to *glyceraldehyde 3-phosphate dehydrogenase* (*GAPDH*).

HMMR constructs expression in MEFs

HEK293FT cells were transfected using Lipofectamine 2000 (Invitrogen) with vectors containing *HMMR*^{FL}, *HMMR*$^{1\text{-}623}$, or *HMMR*$^{1\text{-}679}$ for 72 h. Supernatant was collected and concentrated using the Lenti-X concentrator (Clontech). Virus was added to MEFs with polybrene (8 µg/ml). After 24 h, the media were replaced and cells were grown for an additional 24 h prior to imaging.

Transfection

The following siRNAs were used in this study: HMMR and Scrambled siRNA (Chen *et al.*, 2014) and Kif15 SMARTpool (Dharmacon).

Isolation of splenic cells and MEFs

Spleens were collected from 3-mo-old male littermates. Tissues were homogenized and lysed with Tris-ammonium chloride, and the number of spleen cells was measured using a Hemavet blood analyzer (Drew Scientific, FL): *Hmmr*$^{+/+}$, 16×10^6; *Hmmr*$^{tm1a/+}$, 18.8×10^6; and *Hmmr*$^{tm1a/tm1a}$, 23×10^6.

MEFs were isolated from embryonic day 13.5 mice. Tissues were homogenized using an 18-gauge needle, and cells were seeded and incubated for 2 d, trypsinized on day 3, and frozen once confluent.

MEFs and splenic cells were cultured in DMEM supplemented with 10% FBS (Invitrogen), 4 mM L-glutamax, and 0.1 mM Non-Essential Amino Acids (Invitrogen). For all experiments, MEFs were cultured for only two passages after thawing.

Preparation of chromosome spreads

Cells were treated with 0.05 μg/ml colcemid for 6 h at 37°C and then removed from media. Cells were resuspended in 0.075 M KCl hypotonic solution for 20 min at 37°C. Cells were fixed using cold Carnoy's solution (3 parts methanol: 1 part glacial acetic acid, made fresh) and dropped onto cold glass slides precoated with cold Carnoy's solution. Chromosomes were stained with Hoechst.

Data analysis

Bar graphs display the mean ± SD. All box-and-whisker plots display the median flanked by the 10th, 25th, 75th, and 90th percentiles, and the + sign marks the mean. Statistical analysis was performed by unpaired two-tailed Student's *t* test or one-way analysis of variance (ANOVA) followed by Bonferroni test, with *p* value indicated.

ACKNOWLEDGMENTS

These studies were supported by a BC/Yukon Canadian Breast Cancer Foundation operating grant (C.A.M.), Canadian Institutes for Health Research, in partnership with the Avon Foundation for Women, operating grant (OBC 134038) (C.A.M.), a CIHR New Investigator Salary Award (C.A.M.), a Michael Cuccione Foundation studentship (H.C.) and fellowship (M.C.), and BCCHR scientist level 1 salary awards (C.A.M. and G.S.D.R.).

REFERENCES

Alushin GM, Ramey VH, Pasqualato S, Ball DA, Grigorieff N, Musacchio A, Nogales E (2010). The Ndc80 kinetochore complex forms oligomeric arrays along microtubules. Nature 467, 805–810.

Amato A, Schillaci T, Lentini L, Di Leonardo A (2009). CENPA overexpression promotes genome instability in pRb-depleted human cells. Mol Cancer 8, 119.

Balchand SK, Mann BJ, Titus J, Ross JL, Wadsworth P (2015). TPX2 inhibits Eg5 by interactions with both motor and microtubule. J Biol Chem 290, 17367–17379.

Blangy A, Lane HA, D'Hérin P, Harper M, Kress M, Niggt EA (1995). Phosphorylation by p34cdc2 regulates spindle association of human Eg5, a kinesin-related motor essential for bipolar spindle formation in vivo. Cell 83, 1159–1169.

Bohers E, Sarafan-Vasseur N, Drouet A, Paresy M, Latouche J-B, Flaman J-M, Sesboüé R, Frebourg T (2008). Gradual reduction of BUBR1 protein levels results in premature sister-chromatid separation then in aneuploidy. Hum Genet 124, 473–478.

Chen H, Mohan P, Jiang J, Nemirovsky O, He D, Fleisch MC, Niederacher D, Pilarski LM, Lim CJ, Maxwell CA (2014). Spatial regulation of Aurora A activity during mitotic spindle assembly requires RHAMM to correctly localize TPX2. Cell Cycle 13, 2248–2261.

Chmátal L, Yang K, Schultz RM, Lampson MA (2015). Spatial regulation of kinetochore microtubule attachments by destabilization at spindle poles in meiosis I. Curr Biol 25, 1835–1841.

Chu TLH, Connell M, Zhou L, He Z, Won J, Chen H, Rahavi SMR, Mohan P, Nemirovsky O, Fotovati A, *et al.* (2018). Cell cycle-dependent tumor engraftment and migration are enabled by Aurora A. Mol Cancer Res 16, 16–31.

Ciferri C, Pasqualato S, Screpanti E, Varetti G, Santaguida S, Dos Reis G, Maiolica A, Polka J, De Luca JG, De Wulf P, *et al.* (2008). Implications for kinetochore-microtubule attachment from the structure of an engineered Ndc80 Complex. Cell 133, 427–439.

Collin P, Nashchekina O, Walker R, Pines J (2013). The spindle assembly checkpoint works like a rheostat rather than a toggle switch. Nat Cell Biol 15, 1378–1385.

Connell M, Chen H, Jiang J, Kuan CW, Fotovati A, Chu TL, He Z, Lengyell TC, Li H, Kroll T, *et al.* (2017). HMMR acts in the PLK1-dependent spindle positioning pathway and supports neural development. Elife 6, e28672.

Daum JR, Potapova TA, Sivakumar S, Daniel JJ, Flynn N, Rankin S, Gorbsky GJ (2012). Cohesion fatigue induces chromatid separation in cells delayed at metaphase. Curr Biol 21, 1018–1024.

Drechsler H, McHugh T, Singleton MR, Carter NJ, McAinsh AD (2014). The Kinesin-12 Kif15 is a processive track-switching tetramer. Elife 2014, 1–17.

Dunsch AK, Hammond D, Lloyd J, Schermelleh L, Gruneberg U, Barr FA (2012). Dynein light chain 1 and a spindle-associated adaptor promote dynein asymmetry and spindle orientation. J Cell Biol 198, 1039–1054.

Eibes S, Gallisà-Suñé N, Rosas-Salvans M, Martínez-Delgado P, Vernos I, Roig J (2018). Nek9 phosphorylation defines a new role for TPX2 in Eg5-dependent centrosome separation before nuclear envelope breakdown. Curr Biol 28, 121–129.

Ferenz NP, Paul R, Fagerstrom C, Mogilner A, Wadsworth P (2009). Dynein antagonizes eg5 by crosslinking and sliding antiparallel microtubules. Curr Biol 19, 1833–1838.

Gable A, Qiu M, Titus J, Balchand S, Ferenz NP, Ma N, Collins ES, Fagerstrom C, Ross JL, Yang G, Wadsworth P (2012). Dynamic reorganization of Eg5 in the mammalian spindle throughout mitosis requires dynein and TPX2. Mol Biol Cell 23, 1254–1266.

Gorbsky GJ (2013). Cohesion fatigue. Curr Biol 23, R986–R988.

Groen AC, Cameron LA, Coughlin M, Miyamoto DT, Mitchison TJ, Ohi R, Carolina N, Hill C (2004). XRHAMM functions in Ran-dependent microtubule nucleation and pole formation during anastral spindle assembly. Curr Biol 14, 1801–1811.

Howell BJ, McEwen BF, Canman JC, Hoffman DB, Farrar EM, Rieder CL, Salmon ED (2001). Cytoplasmic dynein/dynactin drives kinetochore protein transport to the spindle poles and has a role in mitotic spindle checkpoint inactivation. J Cell Biol 155, 1159–1172.

Joukov V, Groen AC, Prokhorova T, Gerson R, White E, Rodriguez A, Walter JC, Livingston DM (2006). The BRCA1/BARD1 heterodimer modulates ran-dependent mitotic spindle assembly. Cell 127, 539–552.

Kardon JR, Vale RD (2009). Regulators of the cytoplasmic dynein motor. Nat Rev Mol Cell Biol 10, 854–865.

Kashina AS, Baskin RJ, Cole DG, Wedaman KP, Saxton WM, Scholey JM (1996). A bipolar kinesin. Nature 379, 270–272.

Kunitoku N, Sasayama T, Marumoto T, Zhang D, Honda S, Kobayashi O, Hatakeyama K, Ushio Y, Saya H, Hirota T (2003). CENP-A phosphorylation by Aurora-A in prophase is required for enrichment of Aurora-B at inner centromeres and for kinetochore function. Dev Cell 5, 853–864.

Li H, Frappart L, Moll J, Winkler A, Kroll T, Hamann J, Kufferath I, Groth M, Taudien S, Schütte M, *et al.* (2016). Impaired planar germ cell division in the testis caused by dissociation of RHAMM from the spindle results in hypofertility and seminoma. Cancer Res 76, 6382–6395.

Li X, Nicklas RB (1997). Tension-sensitive kinetochore phosphorylation and the chromosome distribution checkpoint in praying mantid spermatocytes. J Cell Sci 110(Pt 5), 537–545.

Ma N, Titus J, Gable A, Ross JL, Wadsworth P (2011). TPX2 regulates the localization and activity of Eg5 in the mammalian mitotic spindle. J Cell Biol 195, 87–98.

Ma N, Tulu US, Ferenz NP, Fagerstrom C, Wilde A, Wadsworth P (2010). Poleward transport of TPX2 in the mammalian mitotic spindle requires dynein, Eg5, and microtubule flux. Mol Biol Cell 21, 979–988.

Mann BJ, Balchand SK, Wadsworth P (2017). Regulation of Kif15 localization and motility by the C-terminus of TPX2 and microtubule dynamics. Mol Biol Cell 28, 65–75.

Manning AL, Compton DA (2008). SnapShot: nonmotor proteins in spindle assembly. Cell 134, 694–694.e1.

Marthiens V, Rujano MA, Pennetier C, Tessier S, Paul-Gilloteaux P, Basto R (2013). Centrosome amplification causes microcephaly. Mol Biol Cell 15, 731–740.

Maxwell CA, Benítez J, Gómez-Baldó L, Osorio A, Bonifaci N, Fernández-Ramires R, Costes SV, Guinó E, Chen H, Evans GJ, *et al.* (2011). Interplay between BRCA1 and RHAMM regulates epithelial apicobasal polarization and may influence risk of breast cancer. PLoS Biol 9, e1001199.

Maxwell CA, Keats JJ, Belch AR, Pilarski LM, Reiman T (2005). Receptor for Hyaluronan-Mediated Motility correlates with centrosome abnormalities in multiple myeloma and maintains mitotic integrity. Cancer Res 65, 850–860.

Maxwell CA, Keats JJ, Crainie M, Sun X, Yen T, Shibuya E, Hendzel M, Chan G, Pilarski LM (2003). RHAMM is a centrosomal protein that interacts with dynein and maintains spindle pole stability. Mol Biol Cell 14, 2262–2276.

McIntosh JR (1991). Structural and mechanical control of mitotic progression. Cold Spring Harb Symp Quant Biol 56, 613–619.
Neumann B, Walter T, Hériché JK, Bulkescher J, Erfle H, Conrad C, Rogers P, Poser I, Held M, Liebel U, *et al.* (2010). Phenotypic profiling of the human genome by time-lapse microscopy reveals cell division genes. Nature 464, 721–727.
Niault T, Hached K, Sotillo R, Sorger PK, Maro B, Benezra R, Wassmann K (2007). Changing Mad2 levels affects chromosome segregation and spindle assembly checkpoint control in female mouse meiosis I. PLoS One 2, e1165.
Pujana MA, Han JD, Starita LM, Stevens KN, Tewari M, Ahn JS, Rennert G, Moreno V, Kirchhoff T, Gold B, *et al.* (2007). Network modeling links breast cancer susceptibility and centrosome dysfunction. Nat Genet 39, 1338–1349.
Sawin KE, LeGuellec K, Philippe M, Mitchison TJ (1992). Mitotic spindle organization by a plus-end-directed microtubule motor. Nature 359, 540–543.
Scrofani J, Sardon T, Meunier S, Vernos I (2015). Microtubule nucleation in mitosis by a RanGTP-dependent protein complex. Curr Biol 25, 131–140.
Sharp DJ, Brown HM, Kwon M, Rogers GC, Holland G, Scholey JM (2000). Functional coordination of three mitotic motors in Drosophila embryos. Mol Biol Cell 11, 241–253.
Sturgill EG, Das DK, Takizawa Y, Shin Y, Collier SE, Ohi MD, Hwang W, Lang MJ, Ohi R (2014). Kinesin-12 Kif15 targets kinetochore fibers through an intrinsic two-step mechanism. Curr Biol 24, 2307–2313.
Tanenbaum ME, Macůrek L, Galjart N, Medema RH (2008). Dynein, Lis1 and CLIP-170 counteract Eg5-dependent centrosome separation during bipolar spindle assembly. EMBO J 27, 3235–3245.
Tanenbaum ME, Macůrek L, Janssen A, Geers EF, Alvarez-Fernández M, Medema RH (2009). Kif15 cooperates with Eg5 to promote bipolar spindle assembly. Curr Biol 19, 1703–1711.
Uteng M, Hentrich C, Miura K, Bieling P, Surrey T (2008). Poleward transport of Eg5 by dynein-dynactin in Xenopus laevis egg extract spindles. J Cell Biol 182, 715–726.
van Heesbeen RGHP, Tanenbaum ME, Medema RH (2014). Balanced activity of three mitotic motors is required for bipolar spindle assembly and chromosome segregation. Cell Rep 8, 948–956.
Wang H-W, Long S, Ciferri C, Westermann S, Drubin D, Barnes G, Nogales E (2008). Architecture and flexibility of the yeast Ndc80 kinetochore complex. J Mol Biol 383, 894–903.
Wittmann T, Boleti H, Antony C, Karsenti E, Vernos I (1998). Localization of the kinesin-like protein Xklp2 to spindle poles requires a leucine zipper, a microtubule-associated protein, and dynein. J Cell Biol 143, 673–685.
Wittmann T, Wilm M, Karsenti E, Vernos I (2000). TPX2, a novel xenopus MAP involved in spindle pole organization. J Cell Biol 149, 1405–1418.
Wojcik E, Basto R, Serr M, Scaërou F, Karess R, Hays T (2001). Kinetochore dynein: its dynamics and role in the transport of the Rough deal checkpoint protein. Nat Cell Biol 3, 1001–1007.
Ye AA, Deretic J, Hoel CM, Hinman AW, Cimini D, Welburn JP, Maresca TJ (2015). Aurora A kinase contributes to a pole-based error correction pathway. Curr Biol 25, 1842–1851.